

**DEVELOPMENT OF $\text{La}_{0.5}\text{Sr}_{0.5}\text{Co}_{0.95}\text{Nb}_{0.05}\text{O}_{3-\delta}$ AND
 $\text{Sr}_2\text{CoNbO}_{6-\delta}$ CATHODES FOR OXYGEN REDUCTION
REACTION IN SOLID OXIDE FUEL CELL**

VICKY RAHUL DHONGDE



**DEPARTMENT OF CHEMICAL ENGINEERING
INDIAN INSTITUTE OF TECHNOLOGY DELHI
DECEMBER 2024**

© Indian Institute of Technology Delhi (IITD), New Delhi, 2024

**DEVELOPMENT OF $\text{La}_{0.5}\text{Sr}_{0.5}\text{Co}_{0.95}\text{Nb}_{0.05}\text{O}_{3-\delta}$ AND
 $\text{Sr}_2\text{CoNbO}_{6-\delta}$ CATHODES FOR OXYGEN REDUCTION
REACTION IN SOLID OXIDE FUEL CELL**

by

VICKY RAHUL DHONGDE

DEPARTMENT OF CHEMICAL ENGINEERING

Submitted

In fulfilment of the requirements of the degree of

DOCTOR OF PHILOSOPHY

to the



INDIAN INSTITUTE OF TECHNOLOGY DELHI

DECEMBER 2024

*Dedicated to my parental grandmother Smt. Gangubai
Arjun Dhongde, maternal grandmother Smt. Nanda
Bhanudas Jamgade and parents*

Certificate

This is to certify that the thesis entitled “**Development of $\text{La}_{0.5}\text{Sr}_{0.5}\text{Co}_{0.95}\text{Nb}_{0.05}\text{O}_{3-\delta}$ And $\text{Sr}_2\text{CoNbO}_{6-\delta}$ Cathodes for Oxygen Reduction Reaction in Solid Oxide Fuel Cell**” submitted by **Mr. Vicky Rahul Dhongde** to the Indian Institute of Technology Delhi, for the award of the degree of Doctor of Philosophy, is a record of the original bonafide research work carried out by him. He has worked under my supervision and has fulfilled the requirements, which, to my knowledge, has reached the requisite standard for the submission of this thesis. The results contained in this thesis have not been submitted in part or full to any University or Institute for the award of any degree or diploma.



Prof. Siddhasatwa Basu
Supervisor
Department of Chemical Engineering
Indian Institute of Technology Delhi



Prof. M Ali Haider
Supervisor
Department of Chemical Engineering
Indian Institute of Technology Delhi

Acknowledgements

This experience was truly unforgettable and will forever hold a significant place in my life. I would like to express my deep gratitude to the individuals who played a crucial role in the completion of this thesis. Without their invaluable contributions, this work would not have been possible. I am grateful for the opportunity to express my appreciation for all of them.

First, I am incredibly grateful for the chance to pursue a PhD at IIT Delhi. I want to express my heartfelt appreciation to my supervisors, Prof. Suddhasatwa Basu and Prof. M. Ali Haider at the Chemical Engineering Department, IIT Delhi, for their exceptional guidance in my project. It has been a great pleasure working together with both advisors. Their guidance, encouragement, motivation, and enthusiasm for research have been instrumental in my progress and have boosted my confidence and determination to successfully complete this project. I appreciate their ability to provide constructive criticism while also expressing admiration.

I would like to express my gratitude to the members of my review committee, Prof. Anupam Shukla, Prof. Anil Verma and Prof. Praveen Ingole, for their invaluable suggestions and necessary guidance on technical matters throughout my research work. I would like to express my gratitude to all the faculty members for their invaluable assistance and unwavering support whenever I required it.

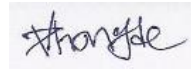
I would like to express my gratitude to the administrative and technical staff members of the Department of Chemical Engineering at the Indian Institute of Technology, Delhi, for their invaluable assistance and cooperation. I would like to express my gratitude to the Nanoscale Research Facility (NRF) and Central Research Facility (CRF) members for their invaluable support in facilitating my research work.

I would like to extend my sincere gratitude to the esteemed individuals who have provided me with invaluable scientific guidance throughout my research journey. Their constant support and expertise have greatly enhanced the cordiality of my work. I am deeply thankful to Dr. Pankaj Tiwari, Dr. Imteyaz Alam, Dr. Tuhin Khan, Dr. Uzma Anjum, Dr. Shahid, Dr. Ajay Kumar, Dr. Rishabh Shukla, Dr. Aditya Singh, Dr. Biswajit De, Dr. Ram Ji Dixit, Dr. Muthuraja, Ms. Priyanka Gupta, Mr. Ajinkya Kotkar, Mr. Venkanna and Dr. Sarath Kumar for their continuous assistance. I would like to express my gratitude to Mr. Sunder Singh for his efforts in making the Fuel cell Lab more accessible and for always being there to assist me whenever I needed help. I want to express my heartfelt gratitude to my friends Dr. Mohit Tiwari, Utsav Dalal, Faisal Khan, Akshit Agrawal, Ankit Patidar and Priyank Rajput for their invaluable assistance, unwavering encouragement, and constant motivation.

I want to express my utmost love and respect for my parents, Rahul Dhongde and Kirti Dhongde, as well as my admiration for my brother, Dr. Nikhil Rahul Dhongde.

I would like to extend my heartfelt gratitude to all those who assisted in the different phases of this project. Unfortunately, I am unable to mention their names due to space constraints.

Finally, I am grateful for the divine power that has provided me with the spiritual strength and bravery to complete this task.



Vicky Rahul Dhongde

Abstract

Over the past few decades, there have been numerous initiatives focused on addressing the energy and environmental challenges caused by the overuse of fossil fuels. SOFC is a highly promising technology among the many proposed solutions. A primary objective of ongoing fuel cell research is to lower the operating temperature of SOFCs. There are several advantages to reducing the operating temperature to a moderate range of 500–800°C. This contributes to the prevention of undesired reactions among the various components of the cell, enhances the overall longevity of the stack, and ultimately results in cost savings. The perovskite material, known as strontium-doped lanthanum cobaltite ($\text{La}_{1-x}\text{Sr}_x\text{CoO}_{3-\delta}$, LSC), has attracted considerable attention due to its remarkable electrocatalytic activity in oxygen reduction. However, the presence of Sr segregation on the surface creates difficulty in oxygen surface exchange, resulting in a decrease in the activity of oxygen ions. The thermal stability of the structure was improved by doping the B-site with a high valent element, Nb, to prevent Sr segregation. $\text{La}_{0.5}\text{Sr}_{0.5}\text{Co}_{0.95}\text{Nb}_{0.05}\text{O}_{3-\delta}$ exhibited a higher oxygen ion diffusion rate of $1.407 \times 10^{-8} \text{ cm}^2 \text{ s}^{-1}$ at a temperature of 973 K compared to $\text{La}_{0.5}\text{Sr}_{0.5}\text{CoO}_{3-\delta}$, which had a diffusion rate of $7.751 \times 10^{-9} \text{ cm}^2 \text{ s}^{-1}$. The results suggest that Nb doping has a positive impact on the diffusion of oxygen ions and improves the structural and thermal stability. The operation of the symmetric solid oxide fuel cell entails supplying H_2 on the anode side and exposing it to air on the cathode side. At a temperature of 700°C, a peak power density of 0.390 W cm^{-2} was observed.

Moreover, the double perovskite structure of $\text{Sr}_2\text{CoNbO}_{6-\delta}$ (SCNO) was prepared to study bulk diffusion. The SCNO demonstrated an impressive peak power density of 0.633 W cm^{-2} at 700°C. The cell was constructed using a pulsed laser deposition technique, resulting in the formation of a dense thin film with thicknesses of 40 nm and 80 nm. The measured polarization

resistance (R_p) for the 40 nm thin film is $0.241 \Omega \text{ cm}^2$, which is actually lower than the R_p of the 80 nm dense thin film at 700°C , which is $0.438 \Omega \text{ cm}^2$.

Furthermore, the composite formation with SDC enhances TEC, conductivity and oxygen vacancy concentration compared to pure SCNO. The SCNO-SDC has excellent electrocatalytic properties, illustrating a lower ASR than the pure SCNO. SCNO-SDC has exceptional resistance to high levels of CO_2 in air atmospheres containing 1-10% CO_2 . At 700°C , the peak power density of SCNO-SDC is 0.786 W/cm^2 with an ASR of $0.085 \Omega/\text{cm}^2$ more than the 0.602 W/cm^2 with an ASR of $0.254 \Omega/\text{cm}^2$ for the SCNO alone.

Furthermore, a comparative study was conducted on three different structural assemblies to analyze the effect of structural modification on the electrochemical performance of SCNO-SDC cathode material. The synthesis of SCNO-SDC cathode materials involves three distinct techniques: mixing, one-pot synthesis, and electrospinning. The electrochemical performance results indicate that the modified structure, specifically the nanofiber composite, demonstrated enhanced ORR activity and lower ASR compared to conventional mixed and one-pot composite materials. The EIS results in the DRT analysis indicate that the ORR rate in the structurally modified SCNO-SDC material is affected by oxygen adsorption-dissociation. The nanofiber composite SCNO-SDC cathode in SOFC achieves a maximum peak power density of $0.996 \text{ W}\cdot\text{cm}^{-2}$ at 700°C . In comparison, the one-pot composite and mixed composite SCNO-SDC cathodes exhibit lower maximum peak power densities of $0.831 \text{ W}\cdot\text{cm}^{-2}$ and $0.706 \text{ W}\cdot\text{cm}^{-2}$, respectively. The polarization resistance values for the nanofiber composite, one-pot composite, and mixed composite SCNO-SDC are $0.079 \Omega \text{ cm}^{-2}$, $0.0908 \Omega \text{ cm}^{-2}$, and $0.206 \Omega \text{ cm}^{-2}$, respectively.

Furthermore, co-sputtering techniques to fabricate electrodes were examined for their potential application in IT-SOFC. The stability of two co-sputtered electrodes was compared in the

comparative study: one that was created from the SCNO and Sm/Ce metal alloy (SCNO-SDC) and another that was composed of the SCNO-SDC one-pot composite and a Sm/Ce metal alloy. It exhibited a polarization resistance of $0.142 \Omega \text{ cm}^2$, which remained relatively consistent. In contrast, the SCNO-SDC co-sputtered cathode exhibited a polarization resistance of $0.257 \Omega \text{ cm}^2$ at 700°C , which increased over time. The electrochemical activity toward the ORR is significantly higher when the SCNO-SDC one-pot composite cathode material is co-sputtered compared to the prepared SCNO cathode. In general, the investigation prioritizes the engineering of cathode material and the development of strategies to improve the electrochemical performance of IT-SOFC.

सार

पिछले कुछ दशकों में, जीवाश्म ईंधन के अति प्रयोग के कारण होने वाली ऊर्जा और पर्यावरणीय चुनौतियों को दूर करने पर केंद्रित कई पहल हुई हैं। SOFC कई प्रस्तावित समाधानों में से एक अत्यधिक आशाजनक तकनीक है। चल रहे ईंधन सेल अनुसंधान का एक प्राथमिक उद्देश्य एसओएफसी के ऑपरेटिंग तापमान को कम करना है। ऑपरेटिंग तापमान को 500-800°C की मध्यम सीमा तक कम करने के कई फायदे हैं। यह सेल के विभिन्न घटकों के बीच अवांछित प्रतिक्रियाओं की रोकथाम में योगदान देता है, स्टैक की समग्र दीर्घायु को बढ़ाता है, और अंततः लागत बचत में परिणाम देता है। स्ट्रोंटियम डोपड लैंथेनम कोबाल्टाइट ($\text{La}_{1-x}\text{Sr}_x\text{CoO}_{3-\delta}$, LSC) के रूप में जानी जाने वाली पेरोव्स्काइट सामग्री ने ऑक्सीजन की कमी में अपनी उल्लेखनीय इलेक्ट्रोकेटलिटिक गतिविधि के कारण काफी ध्यान आकर्षित किया है। हालांकि, सतह पर सीनियर अलगाव की उपस्थिति सतह विनिमय तंत्र के लिए एक चुनौती पैदा करती है, जिसके परिणामस्वरूप ऑक्सीजन आयनों की गतिविधि में कमी आती है। Sr अलगाव को रोकने के लिए एक उच्च वैलेंट तत्व, Nb के साथ बी-साइट को डोपिंग करके संरचना की थर्मल स्थिरता में सुधार किया गया था। $\text{La}_{0.5}\text{Sr}_{0.5}\text{Co}_{0.95}\text{Nb}_{0.05}\text{O}_{3-\delta}$ ने $\text{La}_{0.5}\text{Sr}_{0.5}\text{CoO}_{3-\delta}$ की तुलना में 973 K के तापमान पर $1.407 \times 10^{-8} \text{ cm}^2 \text{ s}^{-1}$ की उच्च ऑक्सीजन आयन प्रसार दर प्रदर्शित की, जिसकी प्रसार दर $7.751 \times 10^{-9} \text{ cm}^2 \text{ s}^{-1}$ थी। परिणाम बताते हैं कि Nb डोपिंग का ऑक्सीजन आयनों के प्रसार पर सकारात्मक प्रभाव पड़ता है और संरचनात्मक और थर्मल स्थिरता में सुधार होता है। सममित ठोस ऑक्साइड ईंधन सेल के संचालन में एनोड पक्ष पर H_2 की आपूर्ति होती है और इसे कैथोड पक्ष पर हवा में उजागर किया जाता है। 700°C के तापमान पर, 0.390 W cm^{-2} का शिखर शक्ति घनत्व देखा गया। इसके अलावा, $\text{Sr}_2\text{CoNbO}_{6-\delta}$ (SCNO) की डबल पेरोव्स्काइट संरचना थोक प्रसार का अध्ययन करने के लिए तैयार की गई थी। SCNO ने 0.633 W cm^{-2} 700°C की प्रभावशाली शिखर शक्ति घनत्व का प्रदर्शन किया। सेल का निर्माण एक स्पंदित लेजर जमाव तकनीक का उपयोग करके किया गया था, जिसके परिणामस्वरूप 40 nm और 80 nm की मोटाई के साथ

घनी पतली फिल्म का निर्माण हुआ। 40 nm पतली फिल्म के लिए मापा ध्रुवीकरण प्रतिरोध (R_p) $0.241 \Omega \text{ cm}^2$ है, जो वास्तव में 700°C पर 80 nm घने पतली फिल्म के प्रतिरोध से कम है, जो $0.438 \Omega \text{ cm}^2$ है।

इसके अलावा, SDC के साथ समग्र गठन शुद्ध एससीएनओ की तुलना में TEC, चालकता और ऑक्सीजन रिक्ति एकाग्रता को बढ़ाता है। SCNO-SDC में उत्कृष्ट इलेक्ट्रोकेटलिटिक गुण हैं, जो शुद्ध एससीएनओ की तुलना में कम Sr को दर्शाते हैं। SCNO-SDC में 2-1% CO_2 युक्त वायु वातावरण में CO_2 के उच्च स्तर के लिए असाधारण प्रतिरोध है। 700°C पर, SCNO-SDC का पीक पावर घनत्व 0.786 W/cm^2 है, जिसमें $0.085 \Omega/\text{cm}^2$ का ASR 0.602 W/cm^2 से $0.254 \Omega/\text{cm}^2$ है, जिसमें अकेले SCNO के लिए $0.254 /\text{cm}^2$ का ASR है।

इसके अलावा, SCNO-SDC कैथोड सामग्री के विद्युत रासायनिक प्रदर्शन पर संरचनात्मक संशोधन के प्रभाव का विश्लेषण करने के लिए तीन अलग-अलग संरचनात्मक विधानसभाओं पर एक तुलनात्मक अध्ययन किया गया था। SCNO-SDC कैथोड सामग्री के संश्लेषण में तीन अलग-अलग तकनीकें शामिल हैं: मिश्रण, एक-पॉट संश्लेषण और इलेक्ट्रोस्पिनिंग। इलेक्ट्रोकेमिकल प्रदर्शन के परिणामों से संकेत मिलता है कि संशोधित संरचना, विशेष रूप से नैनोफाइबर समग्र, ने पारंपरिक मिश्रित और एक-पॉट मिश्रित सामग्री की तुलना में बढ़ी हुई ORR गतिविधि और कम ASR का प्रदर्शन किया। DRT विश्लेषण में ईआईएस परिणाम इंगित करते हैं कि संरचनात्मक रूप से संशोधित SCNO-SDC सामग्री में ORR दर ऑक्सीजन सोखना-पृथक्करण से प्रभावित होती है। SOFC में नैनोफाइबर समग्र SCNO-SDC कैथोड $0.996 \text{ W}\cdot\text{cm}^{-2}$ 700°C की अधिकतम शिखर शक्ति घनत्व प्राप्त करता है। इसकी तुलना में, एक-पॉट समग्र और मिश्रित समग्र SCNO-SDC कैथोड क्रमशः 0.831 W cm^{-2} और 0.706 Wcm^{-2} की कम अधिकतम शिखर शक्ति घनत्व प्रदर्शित करते हैं। नैनोफाइबर समग्र, एक-पॉट समग्र, और मिश्रित समग्र SCNO-SDC के लिए ध्रुवीकरण प्रतिरोध मान क्रमशः $0.079 \Omega \text{ cm}^{-2}$, $0.0908 \Omega \text{ cm}^{-2}$, और $0.206 \Omega \text{ cm}^2$ हैं।

इसके अलावा, IT-SOFC में इसके संभावित अनुप्रयोग के लिए एक सह-स्पट्टिंग, एक उपन्यास इलेक्ट्रोड निर्माण तकनीक की जांच की गई थी। तुलनात्मक अध्ययन में दो सह-स्पट्टर्ड इलेक्ट्रोड की स्थिरता की तुलना की गई थी: एक जो SCNO और Sm/Ce धातु मिश्र धातु (SCNO-SDC) से बनाया गया था और दूसरा जो SCNO-SDC वन-पॉट कम्पोजिट और Sm/Ce धातु मिश्र धातु से बना था। इसने $0.142 \Omega \text{ cm}^2$ के ध्रुवीकरण प्रतिरोध का प्रदर्शन किया, जो समय के साथ अपेक्षाकृत सुसंगत रहा। इसके विपरीत, SCNO-SDC सह-स्पट्टर्ड कैथोड ने $0.257 \Omega \text{ cm}^2$ 700°C का ध्रुवीकरण प्रतिरोध प्रदर्शित किया, जो समय के साथ बढ़ता गया। ORR की ओर विद्युत रासायनिक गतिविधि काफी अधिक होती है जब SCNO-SDC एक-पॉट समग्र कैथोड सामग्री अकेले SCNO कैथोड का उपयोग करने की तुलना में सह-स्पट्टिंग होती है। सामान्य तौर पर, जांच ने कैथोड सामग्री की इंजीनियरिंग और IT-SOFC के विद्युत रासायनिक प्रदर्शन में सुधार के लिए रणनीतियों के विकास को प्राथमिकता दी।

Table of contents

Title	Page No.
Certificate	i
Acknowledgements	ii
Abstract	iv
संर	vii
Table of contents	x
List of figures	xiv
List of tables	xxii
Chapter 1: Introduction	1-21
1.1 Solid oxide fuel cell	3
1.1.1 Configuration and components of solid oxide fuel cell	5
1.1.2 Electrolyte	6
1.1.3 Anode	7
1.1.4 Cathode	7
1.2 Oxygen reduction reaction at the cathode	8
1.2.1 Design cathode for ORR	13
1.3 Motivation for the present work	17
1.4 Scope and objectives of the thesis	19
1.5 Thesis organization	20
Chapter 2: Literature Survey	22-35
2.1 Introduction	22
2.2 Perovskites and its composites	23
2.2.1 Simple perovskites	23

2.2.2 Double perovskite	28
2.3 Research gaps and scope of the thesis	33
Chapter 3: Experimental method	36-60
3.1 Introduction	36
3.2 Materials and its properties	36
3.3 Material synthesis procedure	37
3.3.1 Combustion synthesis route	37
3.3.1.1 $\text{La}_{0.5}\text{Sr}_{0.5}\text{Co}_{0.95}\text{Nb}_{0.05}\text{O}_{3-\delta}$ perovskite	37
3.3.1.2 $\text{Sr}_2\text{CoNbO}_{6-\delta}$ double perovskite	38
3.3.2 Conventional mixed composite	38
3.3.3 One pot composite	39
3.3.4 Nanofiber composite	40
3.4 Fabrication of button cell	41
3.5 Physical and chemical characterizations	45
3.5.1: X-ray Diffraction (XRD) analysis	45
3.5.2 Field emission scanning electron microscopy (FESEM)	46
3.5.3 Energy dispersive x-ray analysis (EDX)	46
3.5.4 High-resolution transmission electron microscopy (HR-TEM)	47
3.5.5 Thermogravimetric analysis (TGA), oxygen non-stoichiometry and oxygen temperature programmed desorption	47
3.5.6 Brunauer-Emmett-Teller (BET) surface area analysis	48
3.6 Electrochemical characterizations	49
3.6.1 Conductivity measurement	49
3.6.2 Fuel cell testing	51

3.6.2.1 Electrochemical impedance spectroscopy and distribution of relaxation time	51
3.6.2.2 Current-Voltage (I-V) characteristic	54
3.6.2.3 Symmetric cell analysis, diffusion and surface exchange coefficient	56
3.7 DFT calculations and molecular dynamic simulations	58
Chapter 4: Radio-frequency magnetron sputtered thin-film $\text{La}_{0.5}\text{Sr}_{0.5}\text{Co}_{0.95}\text{Nb}_{0.05}\text{O}_{3-\delta}$ perovskite electrodes for intermediate temperature symmetric solid oxide fuel cell (IT-SSOFC)	61-75
4.1 Results and discussion	61
4.1.1 Phase analysis, surface morphology and surface composition analysis	61
4.1.2 Oxygen vacancy formation and diffusion coefficient analysis	66
4.1.3 Thermal stability analysis	67
4.1.4 Conductivity and electrochemical analysis	69
4.2 Conclusion	75
Chapter 5: Tailoring the $\text{Sr}_2\text{CoNbO}_{6-\delta}$-$\text{Sm}_{0.2}\text{Ce}_{0.8}\text{O}_{1.9}$ composite to enhance the electrode oxygen reduction kinetics and CO_2 tolerance for IT-SOFC	76-105
5.1 Result and discussion	76
5.1.1 Phase, surface morphology and structural composition analysis	76
5.1.2 Thermal stability and conductivity analysis	79
5.1.3 Diffusion and surface exchange coefficient analysis	83
5.1.4 Symmetric cell measurement	85
5.1.5 Physico-chemical analysis of SCNO-SDC	87
5.1.6 Conductivity, symmetric cell and CO_2 tolerance analysis	92
5.1.7 Full cell and long-term stability analysis	98

5.2 Conclusion	104
Chapter 6: Exploring the impact of structural modification on oxygen reduction reaction in double perovskite composite cathode material for IT-SOFC	106-126
6.1 Result and discussion	106
6.1.1 Phase, surface morphology, structural composition and surface area analysis	106
6.1.2 Diffusion coefficient, surface exchange coefficient and electrochemical analysis	113
6.2 Conclusion	125
Chapter 7: Development of Sr₂CoNbO_{6-δ}-Sm_{0.2}Ce_{0.8}O_{2-δ} cathode using a co-sputtering technique for IT-SOFC	127-135
7.1 Result and discussion	127
7.1.1 Phase analysis	127
7.1.2 Surface morphology and supply power optimization	128
7.1.3 Structural composition and electrochemical analysis	131
7.2 Conclusion	134
Chapter 8: Summary and Future Scope	136-139
8.1 Summary	136
8.2 Future Scope	137
Appendix	140-150
References	151-175
Resume of Author	176-179

List of Figures

Figure No.	Title	Page No.
Figure 1.1	Schematic illustration of SOFC	3
Figure 1.2	Basic design and configurations of SOFC, (a) tubular, (b) planar, (c) electrolyte supported, (d) anode supported, (e) cathode supported cell	6
Figure 1.3	Type of conductors(a) electron conductor cathode (b) MIEC cathode (c) MIEC with electrolyte composite cathode	12
Figure 2.1	Schematic representation of simple perovskite ABO_3	24
Figure 2.2	Schematic representation of double perovskite	29
Figure 3.1	Schematics of the material prepared from the combustion technique	38
Figure 3.2	SCNO-SDC composite prepared using the one-pot synthesis process	40
Figure 3.3	SCNO-SDC nanofiber fabricated using the electrospinning technique	41
Figure 3.4	Schematics of dye set, hydraulic press and high-temperature furnace used for cell fabrication	42
Figure 3.5	Electrolyte-supported cell with cathode	42
Figure 3.6	Anode-supported cell with cathode coating	43
Figure 3.7	Electrode fabrication using the RF sputtering	43
Figure 3.8	Schematic of Pulse laser deposition	44
Figure 3.9	Schematics of electrical conductivity measurement of (a) four probe method anode (b) two probe method, (c) pellet kept in the heating furnace	51

Figure 3.10	Full cell with the silver connection	55
Figure 3.11	Full cell mounted on alumina tube	55
Figure 3.12	Schematics of SOFC testing set-up	56
Figure 3.13	Experimental set-up for studying the diffusion and surface exchange coefficients	57
Figure 4.1	(a) Rietveld refinement of LSCNO perovskite XRD pattern (b) XRD pattern of LSCNO thin film deposited on GDC electrolyte	62
Figure 4.2	FESEM analysis of (a) LSCNO synthesized powder (b) EDX analysis (c) elemental mapping (d – h) elemental distribution Nb, Sr, Co, O, La.	63
Figure 4.3	(a) Microstructural analysis of ~40 nm thin film (b) ~80 nm thin film (c) ~200 nm thin film on GDC electrolyte using RF magnetron sputtering	63
Figure 4.4	XPS spectra of the surface of thin film LSCNO perovskite electrode and corresponding deconvoluted species (a) Co 2p, (b) Nb 3d and (c) O 1s	65
Figure 4.5	$\text{La}_{0.5}\text{Sr}_{0.5}\text{CoO}_3$ and $\text{La}_{0.5}\text{Sr}_{0.5}\text{Co}_{0.95}\text{Nb}_{0.05}\text{O}_3$ structure, where yellow sphere represents vacancy in Sr-O, La-O plane	66
Figure 4.6	Mean square displacement (MSD) plot with time for (a) LSCO and (b) LSCNO	67
Figure 4.7	Coefficient of thermal expansion (a) from dilatometer (b) from molecular dynamic simulation	68
Figure 4.8	Arrhenius plot for (a) ionic conductivity and (b) electrical conductivity of LSCNO estimated experimentally	69

	Electrochemical impedance spectra of symmetric cell (a) brush painted (b) 80 nm (c) 40 nm and (d) Arrhenius plot for temperature-dependant polarization resistance for LSCNO symmetric cells deposited using brush painting and RF magnetron sputtering	72
Figure 4.9		
	(a) Polarization resistance and (b) I-V and I-P curve of symmetric cell LSCNO-GDC-LSCNO measured from 773 K to 973 K in fuel cell mode in the presence of air/H ₂ supply	73
Figure 4.10		
	(a) XRD pattern of SCNO, 40 nm and 80 nm thin film of SCNO deposited over the GDC electrolyte, (b) FESEM image of the SCNO bulk material and the cross-section of a thin film of SCNO on GDC substrate (c) ~80 nm and d. 40 nm.	77
Figure 5.1		
	(a) XPS spectrum of Co 2p and (b) O 1s for SCNO powder and thin films	79
Figure 5.2		
	(a) TGA and oxygen nonstoichiometric of SCNO (b) O ₂ -TPD, (c) Arrhenius plot from ionic conductivity, (d) TEC analysis, (e) H ₂ -TPR, and (f) Arrhenius plot from electronic conductivity	83
Figure 5.3		
	(a) ECR response curve for SCNO bulk material at elevated temperature under the rapid switching of O ₂ partial pressure from 0.1 atm to 0.21 atm (b) Activation energy calculation for bulk diffusion coefficient and surface exchange coefficient for SCNO	84
Figure 5.4		

	Impedance spectra and DRT analysis of (a & d) ~40 nm (b	
Figure 5.5	& e) ~80 nm dense thin film and (c & f) porous electrode of SCNO double perovskite symmetric cell	87
Figure 5.6	(a) XRD pattern of SCNO double perovskite and SCNO- SDC composite, (b) TGA curve, (c) TEC curve,	89
Figure 5.7	(a) and (b) FESEM micrograph, (c) and (d) HRTEM image	90
Figure 5.8	(a) and (b) XPS core-level profile Co and O.	92
Figure 5.9	electrical conductivity of SCNO-SDC and SCNO in air	93
Figure 5.10	(a) and (b) compares the EIS of SCNO and SCNO-SDC composite at 700°C under the various oxygen partial pressure conditions, (c) and (d) DRT plots, (e) and (f) the ASR as a function of oxygen partial pressure for SCNO and SCNO-SDC.	96
Figure 5.11	(a) and (b) EIS of symmetric cells of SCNO-SDC and SCNO under the air atmosphere, exposed to CO ₂ for 120 min and after 60 min of CO ₂ treatment (c) FTIR spectra of SCNO and SCNO-SDC composite after the CO ₂ treatment at 700°C, and (d) Time-dependent polarization with the varying concentration of CO ₂ at 700°C	98
Figure 5.12	(a) and (b) EIS of the SCNO and SCNO-SDC of the full cell (c) and (d) I-P and I-V curve of the full cell	100
Figure 5.13	(a) and (b) Long-term stability of the SCNO-SDC with the cross-section of the full cell and the change in ASR with time, (c) and (d) FESEM and HRTEM of the epitaxially grown SDC particles over the SCNO-SDC composite, (e)	103

	Schematic of SDC particle growth mechanism over SCNO-SDC composite	
Figure 5.14	FESEM and EDAX image of post-mortem analysis of SCNO-SDC one-pot cathode composite	104
Figure 5.15	Post-mortem analysis of SCNO-SDC one-pot composite cathode after symmetric cell analysis	104
Figure 6.1	XRD pattern of SCNO-SDC mixed composites, one-pot, nanofiber composite, and SCNO double perovskite	104
Figure 6.2	(a)FESEM and (b) HRTEM of SCNO-SDC composites surface morphology of mixed composites	108
Figure 6.3	(a)FESEM and (b) HRTEM of SCNO-SDC composites surface morphology of one pot synthesized composites	109
Figure 6.4	(a)FESEM and (b) HRTEM of SCNO-SDC composites surface morphology of electrospun nanofiber composite	110
Figure 6.5	XPS analysis of (a) SCNO-SDC mixed composite, (b) SCNO@SDC one-pot, and (c) nanofiber composite (a) Ce3d (b) Co2p (c) O1s	112
Figure 6.6	(a) Thermogravimetric analysis at air atmosphere and (b) BET surface area analysis and N ₂ adsorption-desorption isotherm SCNO-SDC mixed, one-pot and nanofiber composites in air atmosphere	113
Figure 6.7	The ECR results of (a) SCNO-SDC mixed, (b) one-pot, and (c) nanofiber composite to sudden alteration of partial pressure of oxygen from 0.21 atm (pO ₂) to 0.1 atm (pO ₂ ')	114

Figure 6.8	(a) ASR of the symmetric cell for SCNO-SDC mixed composite, SCNO@SDC one-pot synthesized, nanofiber composite in air atmosphere for the temperature range of 500°C to 700°C (b) Arrhenius plot of polarization resistance for SCNO-SDC composite cathodes, and (c) Comparison of ASRs stability of SCNO-SDC composites in air electrodes	117
Figure 6.9	EIS and DRT and estimated polarisation resistance (R_p) of the symmetric cell at various pO_2 ranged from 0.1 atm to 1 atm at 700°C, (a, b, c) SCNO-SDC mixed composite, (d, e, f) SCNO-SDC one-pot synthesized, (g, h, i) SCNO-SDC nanofiber composite	120
Figure 6.10	(a) Schematic illustration of step associated with ORR, (b) oxygen ion transfer path in SCNO-SDC mixed composite, one-pot synthesized, nanofiber composite.	122
Figure 6.11	(a) I-V-P curve for full cell performance and (b) EIS of the SCNO-SDC mixed composite, SCNO-SDC one-pot synthesized and nanofiber composite as a cathode at 700°C	124
Figure 7.1	XRD pattern of SCNO and SCNO-SDC one-pot target, SCNO-SDC co-sputtered electrode and SCNO-SDC one-pot co-sputtered film over a glass substrate	128
Figure 7.2	FESEM surface morphology of the SCNO-SDC film fabricated using (a) 30 W and (b) 50 W power supplied to Sm/Ce metal alloy target, (c) 150 W, (d) 200 W, and (e) 250 W power supplied to SCNO target	129

Figure 7.3	FESEM cross-section of the electrode films of (a) SCNO-SDC co-sputtering over the SDC substrate and (b) SCNO-SDC one-pot composite fabricated using co-sputtering over the SDC substrate	130
Figure 7.4	XPS analysis of the surface oxidation state of SCNO-SDC one pot and SCNO-SDC electrode fabricated using the co-sputtering process (a) O1s, (b) Co2p and (c) Ce3d	132
Figure 7.5	Electrochemical analysis of symmetric cell electrode fabricated from (a) SCNO-SDC, (b) SCNO-SDC one pot, and (c) comparison of the stability of SCNO-SDC and SCNO-SDC one pot at 700°C	133
Figure 7.6	Full cell performance of the SCNO-SDC one-pot electrode fabricated from co-sputtering (a) I-V-P and (b) EIS	134
Figure 8.1	Schematic illustration of the co-sputtering process for electrode fabrication and its advantages	139
Figure A1	Stability analysis of symmetric solid oxide fuel cell under a current density of 393 mA cm ⁻² at 973 K with H ₂ as fuel and air oxidant	140
Figure A2	Post-mortem analysis of the electrode surface after the course of symmetric solid oxide fuel cell operation	141
Figure A3	Schematic illustration of La _{0.5} Sr _{0.5} Co _{0.95} Nb _{0.05} O _{3-δ} synthesis process	141
Figure A4	XPS spectrum of Sr 3d of SCNO powder and thin film	141
Figure A5	Rietveld refinement of SCNO double perovskite and SCNO-SDC cathode composite	142

Figure A6	FESEM and EDAX image of SCNO double perovskite	144
Figure A7	FESEM and EDAX image of SCNO-SDC one-pot composite cathode	144
Figure A8	XPS spectrum of (a) Sr and (b) Nb associated with SCNO and SCNO-SDC (c) Sm and (d) Ce of SCNO-SDC	145
Figure A9	Surface morphology and elemental mapping (a) to (g) SCNO-SDC mixed composite, (h) to (n) one-pot prepared, (o) to (u) nanofiber composite	147
Figure A10	XPS analysis of (a) Sr3d, (b) Sm3d, and (c) Nb3d for mixed composite, one-pot composite, and nanofiber composite	148
Figure A11	(a) Relationship between SDC content and ASR values for SCNO-SDC composite cathodes (b) Arrhenius plot of ASR values for SCNO-SDC composite cathodes	148
Figure A12	EIS of the symmetric cell for (a) SCNO-SDC mixed composite, (b) one-pot synthesized, (c) nanofiber composite in air atmosphere for the temperature range of 500°C to 700°C	149
Figure A13	Circuit fitting to the Nyquist plot R(CR)(CR)	149
Figure A14	XPS analysis spectra of Sr3d of co-sputtered electrode made from SCNO-SDC and one-pot composite	150

List of Tables

Table No.	Title	Page No.
Table 1.1	Different types of fuel cells	2
Table 2.1	Summary of pure electronic conductors and mixed ionic and electronic conductors (MIECs) simple perovskites conductivities	24
Table 2.2	LSCO-based perovskites ASR with doping at B-site	27
Table 2.3	The conductivity and ASR values of different double perovskites as per the literature	30
Table 3.1	List of chemical compositions of materials used for the preparation of different components of solid oxide fuel cell and their properties and supplier	36
Table 3.2	Interatomic paired Buckingham potentials for LSCNO	59
Table 4.1	XPS curve fitted results for Co 2p and O 1s	65
Table 4.2	Resistance values from the EIS for the temperature range of 673 K to 973 K	72
Table 6.1	Measurement of the oxygen bulk diffusion coefficient and surface exchange coefficient at various temperatures using the ECR technique	114
Table 6.2	Preparation processes and PPD of double perovskite composites at 700°C	124
Table A1	Comparison of R_p of different electrodes for symmetrical solid oxide fuel cell	140
Table A2	D_{chem} and K_{ex} of SCNO material for the temperature range of 500°C to 700°C	142

Table A3	Rietveld refined parameters of $\text{Sr}_2\text{CoNbO}_{6-\delta}$ (SCNO)	142
Table A4	Rietveld refined parameters of $\text{Sr}_2\text{CoNbO}_{6-\delta}\text{-Sm}_{0.2}\text{Ce}_{0.8}\text{O}_{2-\delta}$ (SCNO-SDC)	143
Table A5	The change in lattice volume of SCNO and SCNO-SDC	143
Table A6	Peak power density of double perovskite cathode at 700°C	146
Table A7	ICP-MS composition of the prepared composites	149
